Journal of Applied Electrochemistry **33**: 1069–1075, 2003.

Electrochemical study and complete factorial design of Toluidine Blue immobilized on SiO_2/Sb_2O_3 binary oxide

E.S. RIBEIRO[1], S.L.P. DIAS[1], S.T. FUJIWARA[1], Y. GUSHIKEM[1]* and R.E. BRUNS[1,2]
[1]*Instituto de Química, Unicamp, CP 6154, 13083-970, Campinas, SP, Brazil*
[2]*Instituto de Química, Universidade de São Paulo. CP 26077, 05513-970, São Paulo, SP, Brazil*
*(*author for correspondence, fax: +55 19 3788 3023, e-mail: gushikem@iqm.unicamp.br)*

Received 24 August 2002; accepted in revised form 20 May 2003

Key words: antimonium oxide, carbon paste electrode, factorial design, sol–gel process, Toluidine Blue

Abstract

SiO_2/Sb_2O_3 of specific surface area $S_{BET} = 788\ m^2\ g^{-1}$ and 4.7 wt % of Sb was prepared by the sol–gel method. Toluidine Blue (TB^+) was immobilized on SiO_2/Sb_2O_3 by ion exchange reactions and the amount of dye bonded to the substrate surface was 13.72 μmol g^{-1} for SiO_2/Sb_2O_3. This material was used to modify carbon paste electrodes and the electrochemical properties of Toluidine Blue (TB^+) immobilized on a silica surface modified with antimonium trioxide were investigated by cyclic voltammetry. The electron mediator property of toluidine blue was optimized using a factorial design, consisting of four factors each at two levels. Factorial analysis was carried out by searching for better reversibility of the redox process, that is, the lowest separation between anodic and cathodic peak potentials and a current ratio near unity. The aqueous phase pH does not appear to influence the peak separation, ΔE, and the $|I_{pa}/I_{pc}|$ current ratio response. The other factors studied, the scan rate, type of electrolyte and electrolyte concentration are important for this chemically modified electrode system demonstrating significant influences on the reversibility of electron transfer. The experimental observations and data analyses on this system indicate that the smallest peak separation occurs using 20 mV s^{-1} and 1.0 mol L^{-1} KCl while values of $|I_{pa}/I_{pc}|$ close to unity are found for 20 mV s^{-1} with 1.0 mol L^{-1} concentrations of either KCl or CH_3COONa. The electrodes presented reproducible responses and were chemically stable for various oxidation-reduction cycles.

1. Introduction

Binary SiO_2/M_xO_y oxides obtained by the sol–gel processing method have found many applications in recent years [1–8] .The materials obtained combine the mechanical properties of the silica matrix with the chemical properties of the bulk metal oxides. The sol–gel process yields a solid with controlled porosity and the metal oxide can be obtained as highly dispersed particles in the matrices [7]. Basically, the procedure consists of the reaction between tetraethylorthosilicate, $Si(OR)_4$, and the metal oxide precursor, $M(OR')_4$:

$$Si(OR)_4 + xM(OR')_y \xrightarrow{\text{solv + acid}} SiO_2/M_xO_y + 4\,ROH + xyR'OH \qquad (1)$$

Growing interest in using these materials as a porous substrate to immobilize electroactive species lies in the possibility of preparing a series of electrochemical sensors (chemically modified electrodes) [1, 9, 10]. Many applications of antimony(III) oxide have been found in recent years as flame-retardants [11–14], as the main component for glass formation [15], as catalysts [16–19] and as an ion exchanger [20, 21].

Toluidine Blue (TB^+) can be immobilized on SiO_2 matrices grafted with TiO_2 and used to prepare modified carbon paste electrodes for use as electrochemical sensors for NADH [22] or the oxalate ion [23]. In these cases the main characteristic was that modified carbon paste electrodes made with immobilized dye material presented a constant midpoint potential in aqueous phases at different pH, in contrast to those observed for dyes in the solution phase [24] or when immobilized on graphite surfaces [25, 26]. The shift of E_m towards more positive values is desirable to enhance the redox reaction and achieve more efficient electrocatalysis [27]. These redox potentials are very close to most of the biomolecular redox potentials and the chemically modified electrodes based on this dye as an electron mediator system may be of great interest for developing biosensors [28, 29]. The efficient optimization of electron transfer between Toluidine Blue and the electrode is an important step in developing the biosensor.

In the present work, the electrochemical properties of TB^+ immobilized on SiO_2/Sb_2O_3 mixed oxide matrix,

prepared by the sol–gel method, are described. The study of immobilized dye in the pores of solid matrices presenting high specific surface areas such as those used in this work is important for developing a new class of sensors [9,30] aimed at achieving higher sensitivity, selectivity and stability. The preparation of silica modified with antimonium trioxide for surface immobilization of toluidine blue is reported. The optimization of this system was carried out by searching for the best reversibility characteristics of the adsorbed mediator using a two level-four variable factorial design [31, 32]. Statistical methods of experimental design and systematic optimization such as factorial designs have been applied to different chemical systems [31–36], owing to their capabilities of extracting relevant information from systems while requiring a minimum number of experiments.

2. Experimental details

2.1. *Preparation of SiO_2/Sb_2O_3 mixed oxide*

The SiO_2/Sb_2O_3 mixed oxide was prepared according to the following procedure: To 210 ml of a 50% (v/v) solution of ethanol/TEOS (TEOS, tetraethylorthosilicate), 12 ml of 3.5 mol L^{-1} HCl were added. The mixture was stirred for 3 h at 333 K. After the prehydrolysis step, 22 g of $SbCl_3$ were added and the mixture stirred for 3 h at room temperature. An additional 6.0 ml of 3.5 mol L^{-1} HCl solution was added and the mixture stirred for another 2 h at room temperature. The solvent was slowly evaporated at 333 K until gel formation. The gel obtained was ground and sieved between 60 and 200 mesh and the resulting particles washed with ethanol in a soxhlet extractor for 8 h. Finally, the material was washed with 250 ml of 0.1 mol L^{-1} HNO_3, bidistilled water, dried under vacuum (1.3×10^{-2} Pa) and stored.

2.2. *Scanning electron microscopy*

A Jeol JSM T300 scanning electron microscope (SEM), equipped with an energy dispersive (EDS) microprobe from NORAN Instruments (model series 2) was used to obtain micrographs of the material. The samples were dispersed on double faced conductive tape placed on a copper support and coated with gold using Balzer (Med 020) equipment.

2.3. *Specific surface area and chemical analysis of SiO_2/Sb_2O_3*

The specific surface areas, S_{BET}, were measured by the BET multipoint technique on a Micromeritics Flowsorb II 2300 apparatus.

The antimony content in SiO_2/Sb_2O_3 was determined by using X-ray fluorescence analysis on a model 5000 spectrometer equipped with a beryllium window from Tracor X-Ray.

2.4. *Toluidine Blue immobilization on SiO_2/Sb_2O_3*

Toluidine Blue (TB^+) (in Scheme 1) was immobilized on the SiO_2/Sb_2O_3 matrix by an ion exchange reaction. About 0.2 g of SiO_2/Sb_2O_3 were added to 20 ml of a 2×10^{-4} mol L^{-1} toluidine blue solution. The mixture was shaken for 30 min, the time required for the system to achieve equilibrium. The changes in the dye concentrations in the solution phase, before and after equilibrium, were measured by spectrophotometry and the amount of incorporated dye, N_f, in the matrices was determined by applying the equation: $N_f = (N_a - N_s)/m$ where N_a and N_s are, respectively, the initial and final mole numbers of dye (equilibrium condition) in solution phase, and m is the mass of the material. The material obtained is labelled SiO_2/Sb_2O_3/TB.

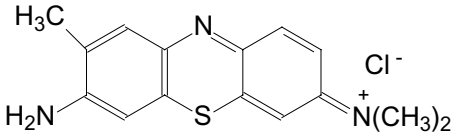

Scheme 1. Structure of Toluidine Blue.

2.5. *UV–visible spectra of the Toluidine Blue on SiO_2/Sb_2O_3*

The UV–visible spectra of the solid samples were obtained as paste in hydrocarbon oil between quartz plates with a 0.01 mm path length. The measurements were carried out on a Beckman DU 640 spectrophotometer. The spectrum of the SiO_2/Sb_2O_3/TB was compared with those of the dyes in aqueous solution.

2.6. *Electrochemical measurements*

The carbon paste electrodes were prepared by mixing the materials (SiO_2/Sb_2O_3 and SiO_2/Sb_2O_3/TB) with analytical grade graphite in 1:1 (weight: weight) proportions with one drop of liquid paraffin as binder. These pastes were placed in a cavity of 1 mm depth, in contact with a platinum disc of 5 mm internal diameter fused to a glass tube. The carbon paste electrodes made with these materials were used as the working electrodes, with a platinum wire serving as the counter electrode and a saturated calomel electrode (SCE) as reference. Cyclic voltammetry studies were carried out using an Autolab PGSTAT 20 potentiostat/galvanostat apparatus. All the measurements were carried out under a pure nitrogen atmosphere in a cell at 298.0 ± 0.2 K. The supporting electrolyte solution pH of KCl was adjusted by adding HCl or KOH. For CH_3COONa, CH_3COOH or NaOH was added.

2.7. *Factorial design*

In this study, a 2^4 full factorial design was used with the aim of determining the importance of one qualitative

Table 1. Factors, levels, peak separation and current ratio response values for the 2^4 factorial design

Runs	Order of experiments	Factors*				ΔE /mV	$\lvert I_{pa}/I_{pc}\rvert$
		1	*2*	*3*	*4*		
1	9	−	−	−	−	83	0.969
2	1	+	−	−	−	152	0.889
3	13	−	+	−	−	156	0.773
4	5	+	+	−	−	267	0.650
5	11	−	−	+	−	51	1.004
6	3	+	−	+	−	84	0.954
7	15	−	+	+	−	80	0.997
8	7	+	+	+	−	134	0.883
9	10	−	−	−	+	77	0.975
10	2	+	−	−	+	142	0.903
11	14	−	+	−	+	169	0.797
12	6	+	+	−	+	279	0.684
13	12	−	−	+	+	51	0.994
14	4	+	−	+	+	84	0.940
15	16	−	+	+	+	85	0.989
16	8	+	+	+	+	141	0.921

*	(−),	(+)
1 Scan rate/mV s^{-1}	20	60
2 Type of electrolyte	KCl,	CH_3COONa
3 [Electrolyte]/mol L^{-1}	0.2,	1.0
4 pH	4.0,	7.0.

Table 2. Main and interaction effects and standard error values for the 2^4 factorial design

Average	ΔE/mV 127.2 ± 1.7	$dI_{pa}/I_{pc}d$ 0.950 ± 0.005
Main effects		
1	66.4 ± 3.3*	−0.08 ± 0.01†
2	73.4 ± 3.3	−0.12 ± 0.01
3	−76.9 ± 3.3	0.13 ± 0.01
4	2.6 ± 3.3	0.01 ± 0.01
Two factor interactions		
12	16.4 ± 3.3	−0.02 ± 0.01
13	−22.4 ± 3.3	0.01 ± 0.01
14	−0.38 ± 3.3	0.008 ± 0.01
23	−30.9 ± 3.3	0.09 ± 0.01
24	6.6 ± 3.3	0.01 ± 0.01
34	0.38 ± 3.3	−0.009 ± 0.01
Three factor interactions		
123	−5.4 ± 3.3	0.008 ± 0.01
124	0.63 ± 3.3	0.007 ± 0.01
134	0.88 ± 3.3	0.003 ± 0.01
234	−3.63 ± 3.3	0.002 ± 0.01
Four factor interactions		
1234	−0.13 ± 3.3	0.006 ± 0.01

*95% confidence interval of ±7.5.
†95% confidence interval of ±0.02.

(electrolyte type) and three quantitative factors (scan rate, aqueous phase pH and electrolyte concentration) on the optimization of the redox process of Toluidine Blue adsorbed on the modified silica surface. The factors chosen for the optimization procedure are those that could affect the reversibility of electron transfer when the mediator is immobilized on the modified silica surface. The factors, their levels and the sixteen experiments of the full 2^4 factorial design are presented in Table 1. The experiments in Table 1 were performed in a random order to avoid possible systematic error being interpreted as significant effect values. Response effects were determined for peak potential separation, ΔE, [$\Delta E = E_{pa} - E_{pc}$ where E_{pa} is the anodic peak potential and E_{pc} is the cathodic peak potential] and as the $|I_{pa}/I_{pc}|$ current ratio. The values of the effects were calculated using equation 2 [32]:

$$Ef_i = \overline{R}_i^{(+)} - \overline{R}_i^{(-)} \quad (2)$$

where $\overline{R}_i^{(+)}$ and $\overline{R}_i^{(-)}$ are the averages of results when the *i*th factor is at its high (+) or low (−) level independent of the signs of the other factor levels. Eight experimental values make up each average because each column in Table 1 has eight positive and eight negative signs. The values of the effects calculated with the data of Table 1 are presented in Table 2.

The statistical significance of all these effects was determined by plotting the effect values on a cumulative probability graphs [31, 32]. Points corresponding to a normal distribution are expected to be located on a line centred about the origin. The effects represented by these points are not significant and correspond to estimates of effect errors. Their values can be used to calculate an estimate of this error as well as the experimental observation error. Effect values were calculated and cumulative probability graphs were plotted using the Factorial [31] and Statistica programs [33].

3. Results and discussion

3.1. *Characterization of the materials*

The SiO_2/Sb_2O_3 binary oxide prepared by the sol–gel method resulted in a highly porous material with a specific surface area of $S_{BET} = 788\ m^2\ g^{-1}$. The amount of Sb incorporated in the binary oxide was 4.7 wt % (0.39 mmol g^{-1}).

Figure 1(a) shows the SEM image for SiO_2/Sb_2O_3 and Figure 1(b) the respective EDS metal mapping image obtained for the Sb atoms. The white points in Figure 1(b) are due to the antimony SbL_α radiation energy at 3.6 keV [37, 38]. From the EDS image the Sb atoms, within the magnification used, are observed to be uniformly dispersed with no detectable phase segregation of the oxide particles in the matrix. This homogeneous dispersion of the metal oxide in the matrix is an important characteristic for material applications.

3.2. *Toluidine Blue immobilization on SiO_2/Sb_2O_3*

Immobilization of Toluidine Blue (Scheme 1) on SiO_2/Sb_2O_3 was done at pH 6.0. Therefore, the form of the immobilized toluidine blue is TB^+.

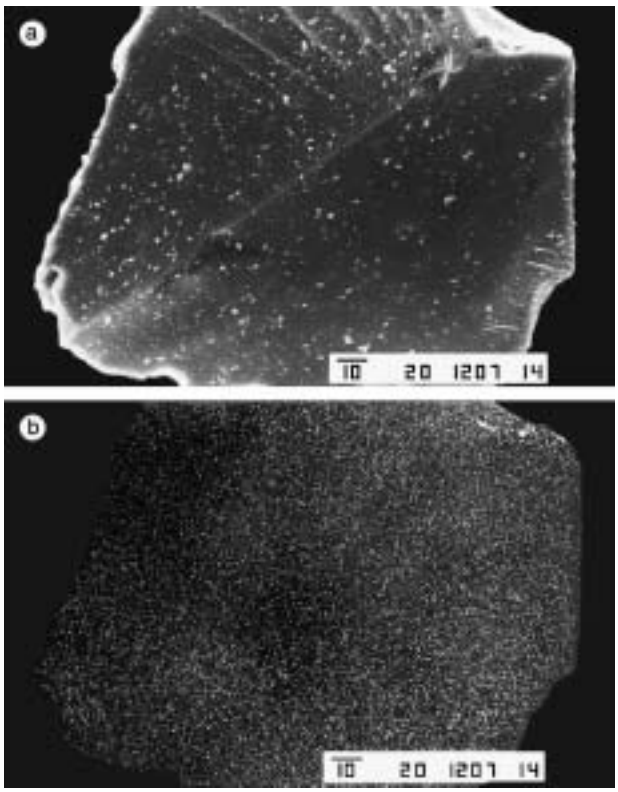

Fig. 1. Scanning electron microscopy image of SiO_2/Sb_2O_3 (a), the corresponding energy dispersive scanning image (EDS) of antimony (b). (scalebar: 10 μm).

The immobilization of Toluidine Blue on the SiO_2/Sb_2O_3 surface occurs by an ion exchange reaction, represented by:

$$SbOH + TB^+ \rightleftharpoons SbOTB + H^+ \quad (3)$$

where SbOH is the Brønsted acid site of the SiO_2/Sb_2O_3 surface.

The amount of dye bonded to the substrate surface was 13.72 μmol g^{-1} for SiO_2/Sb_2O_3.

3.3. *UV–visible spectrum of TB^+ onto SiO_2/Sb_2O_3*

Since the TB^+ can form molecular associations, normally as dimers and sometimes as higher order aggregates, in solution phase [39] and such behavior may persist in the solid phase when TB^+ is adsorbed from aqueous solution on the SiO_2/Sb_2O_3 surface, the UV–visible spectrum of the SiO_2/Sb_2O_3/TB material was obtained and compared with spectra of TB^+ in aqueous solution.

Figure 2(a) shows the spectra for SiO_2/Sb_2O_3/TB and Figure 2(b) the spectra of TB^+ with different concentrations in the solution phase. The peak at the lower wavelengths in both spectra, Figure 2(a) and (b), are due to dimeric species and at the higher wavelengths to monomeric species [40]. The SiO_2/Sb_2O_3/TB material (Figure 2(a)) has one absorption band at 590 nm and a shoulder at 630 nm, indicating a larger predominance of the dimeric species.

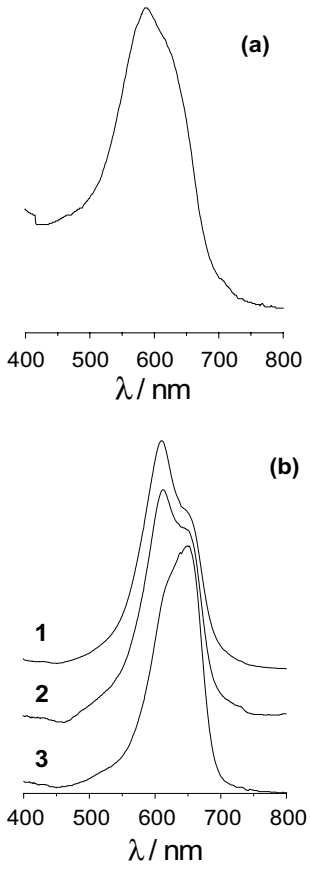

Fig. 2. UV–vis absorption spectra of: (a) SiO_2/Sb_2O_3/TB; (b) TB^+ in aqueous solution: (1) 2.0×10^{-4}, (2) 5.0×10^{-5} and (3) 1.25×10^{-5} mol L^{-1}.

3.4. *Electrochemical studies*

Figure 3(a) and (b) show the cyclic voltammograms of the modified carbon paste electrodes for SiO_2/Sb_2O_3 and SiO_2/Sb_2O_3/TB, respectively. On scanning the potential between −0.4 and 0.1 V vs SCE, no peak currents for SiO_2/Sb_2O_3 modified carbon paste electrode are observed. For the SiO_2/Sb_2O_3/TB modified carbon paste electrode, well-defined anodic and cathodic current densities are observed.

The midpoint potential, E_m, ($E_m = (E_{pa} + E_{pc})/2$ where E_{pa} and E_{pc} are the anodic and cathodic peak potentials) for SiO_2/Sb_2O_3/TB occurs in the region between −150 and −180 mV. The stability of the electrodes was verified by performing several redox cycles, measured in 1.0 mol L^{-1} KCl supporting electrolyte solution, since the species can be leached from the surface of the electrode during several oxidation and reduction cycles. It was observed that up to 80 cycles for the SiO_2/Sb_2O_3/TB electrode, the anodic current density stayed practically constant, even for this high concentration of supporting electrolyte (KCl 1 mol L^{-1}), showing that the dye is not leached from the matrix surface owing to their large affinities. In relation to the cathodic peak current, the same behavior is verified.

Table 1 shows the results of the 2^4 factorial design for the system. The factors chosen for the optimization

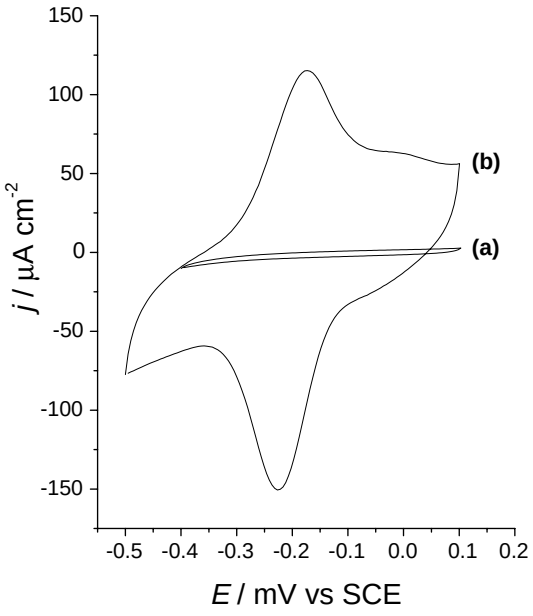

Fig. 3. Cyclic voltammograms obtained for carbon paste electrodes modified with SiO_2/Sb_2O_3 (a) and SiO_2/Sb_2O_3/TB (b). Measurements in 1.0 mol L^{-1} KCl, pH 7.0, $T = 298$ K and scan rate of 20 mV s^{-1}.

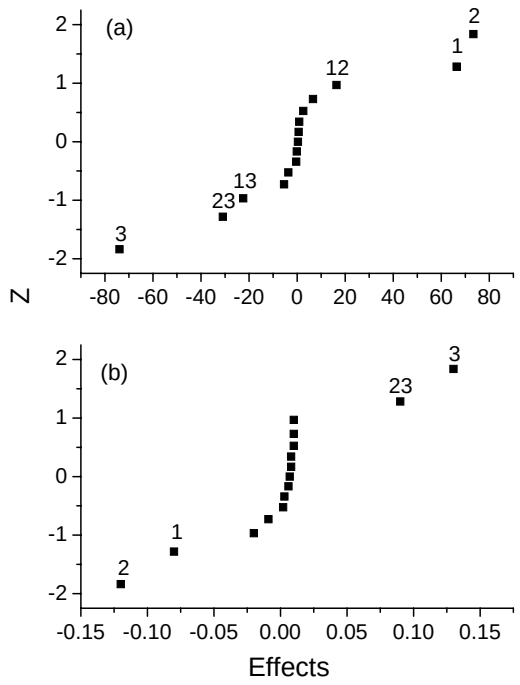

Fig. 4. Cumulative probability graph for the effect values, ΔE (a) and $|I_{pa}/I_{pc}|$ (b), of Table 2 corresponding to the 2^4 factorial design.

procedure are those that could affect the reversibility of electron transfer; scan rate, type of electrolyte, electrolyte concentration and aqueous phase pH to immobilize the mediator. The effects of these factors are presented in Table 2.

For the peak separation response, ΔE, the main effects for scan rate (1) type of electrolyte (2) and electrolyte concentration (3) as well as the binary interactions, scan rate-type of electrolyte (12), scan rate-electrolyte concentration (13) and type of electrolyte–electrolyte concentration (23) have the largest absolute values. For the peak separation response, ΔE, pH has no important effect value. The statistical significance of these effects can be determined by plotting the effect values on a cumulative probability graph [31,32] (Figure 4). This plot shows that the effect values involving pH are not statistically significant.

An estimate of the standard error in the effect values can be obtained by pooling the effect values corresponding to the points linearly distributed about the origin of the cumulative probability graph (Figure 4). This results in an effect standard error of ± 3.3 mV estimated with nine degrees of freedom.

If pH does not really affect peak separation one can expect the results for experiments 1 and 9, 2 and 10... 8 and 16 to be the same within experimental error since these pairs of experiments have identical conditions for the scan rate, type of electrolyte and electrolyte concentration. Inspection of the values in Table 1 confirms this observation.

Comparison of the effect values with their errors and confidence interval uncertainties confirms that for the peak separation response, ΔE, the main effects of scan rate, type of electrolyte and electrolyte concentration, as well as the binary interaction effects (12), (13) and (23), are significant.

For the current ratio response, $|I_{pa}/I_{pc}|$, the main effects involved are scan rate (1) type of electrolyte (2) and electrolyte concentration (3), as well as the binary interaction type of electrolyte-electrolyte concentration (23). Their absolute values are approximately four to six times greater than the values of the other effects, as can be seen in Table 2. An effect standard error of ± 0.01 was estimated by pooling the effect values corresponding to the points on the centerline of the cumulative probability graph for the $|I_{pa}/I_{pc}|$ effect values in Figure 4. Comparison of the corresponding 95% confidence level uncertainties with the effect values in Table 2 shows that the main effects of scan rate, type of electrolyte and electrolyte concentration, as well as the binary interaction effect (23), are significant. Inspection of the values obtained in Table 2 reveals that both the dependence of the peak separation response, ΔE, and current ratio response, $|I_{pa}/I_{pc}|$, are much more complicated than can be described by just three principal effect values alone. Therefore it is more appropriate to investigate these systems using multivariate methods that are capable of measuring binary interaction effects [32].

In Table 1 important trends can be observed. On comparing pairs of experiments that differ only in the sign of factor 1, for example run 1 with 2, 3 with 4 etc., it is possible to see that for all pairs the largest ΔE result occurs when factor 1 is at its high level, that is, this factor has a positive effect. The peak separation values, ΔE, increase with a change in 20 mV s^{-1} scan rate to 60 mV s^{-1}. This is consistent with the positive main

effect value in Table 2 for scan rate. In other words, peak separation response, ΔE, is dependent on scan rate. The absolute value of the peak separation increases to approximately 44.0 mV when the scan rate is changed from 20 to 60 mV s^{-1} and the concentration of the supporting electrolyte is 1.0 mol L^{-1} and this is independent of the aqueous phase pH. Similar behaviour is also observed when the concentration of the electrolyte is 0.2 mol L^{-1}, except that a larger increase of about 88.75 mV in peak separation occurs. This difference of about 44.75 mV (larger than any of the absolute values of the interaction effects) is independent of aqueous phase pH and can be probably attributed to the fact that electron transfer of the mediator is slow, favouring a more reversible system at lower scan rate.

Comparing pairs of experiments that differ only in the sign of factor 2, for example run 1 with 3, 2 with 4 etc., it is possible see that for all pairs the largest ΔE occurs when factor 2 is at its high level, that is, this factor has a positive effect. The peak separation values, ΔE, increase when the inorganic electrolyte KCl is replaced by the organic electrolyte CH_3COON_a. This corresponds to a positive main effect in Table 2 for the type of electrolyte factor. This can be attributed to the smaller ionic mobilities in water at 298 K for CH_3COO^- ($4 \times 24 \times 10^{-8}$ m^2 s^{-1} V^{-1}) and Na^+ ($5 \times 19 \times 10^{-8}$ m^2 s^{-1} V^{-1}) in relation to the Cl^- (7.91×10^{-8} m^2 s^{-1} V^{-1}) and K^+ (7.62×10^{-8} m^2 s^{-1} V^{-1}) [41].

An opposite trend is seen for the electrolyte concentration. Comparing pairs of runs that differ only in the sign of factor 3, runs 1 and 5, 2 and 6 etc., independent of the levels of the other factors, the peak separation values, ΔE are always smaller when the 1.0 mol L^{-1} electrolyte concentration is used instead of 0.2 mol L^{-1}; that is, this factor has a negative effect corresponding to the negative main effect in Table 2 for the electrolyte concentration factor. This is an important characteristic of reversible systems. This behaviour may be attributed to mass transport since the higher the supporting electrolyte concentration the more efficient the electron transfer process is expected to be, thus favoring the largest current response and the smallest separation between peak potentials.

Such tendencies are not observed for the aqueous phase pH, since it does not produce a significant effect.

The binary interaction effect (12) involving the main effect of scan rate and the type of electrolyte is synergistic, that is, the peak separation becomes larger when both factors, scan rate and type of electrolyte are varied simultaneously to their higher levels relative to the sum of increases in peak separation for isolated changes in these factors. In this way, with a simultaneous change in scan rate from 20 to 60 mV s^{-1} and a change of electrolyte from KCl to CH_3COONa an increase in the peak separation of about 16 mV above that owing to the principal effects, 66.4 + 73.4 = 139.8 mV is observed. Two other interaction effects, both antagonistic, one involving the scan rate and electrolyte concentration and the other the type of electrolyte and

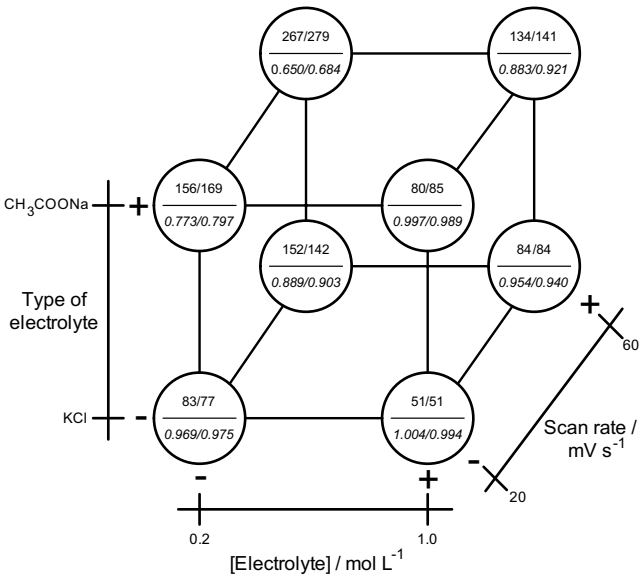

Fig. 5. 2^4 factorial design diagram for the peak separation (arial type) and current ratio (italic type) response values.

electrolyte concentration, are also large and significant [32]. The relatively complex dependence in the peak separation values, ΔE, on these factors can also be analysed using Figure 5. Only multivariate procedures can detect interaction effects. As such, these techniques should be recommended for the study and optimization of chemically modified electrodes.

Examination of the factorial design diagram in Figure 5 confirms the simple behaviour for the ΔE values. The −76.9 mV effect value arises since all ΔE values for the 1.0 mol L^{-1} KCl concentration (right-hand face of cube) are between 29 and 135.5 mV smaller than the corresponding values at 0.2 mol L^{-1} (left-hand face).

Analogously in Figure 5, the positive $|I_{pa}/I_{pc}|$ for the electrolyte concentration effect, 0.13, is a consequence of the fact that ratios on the 1 mol L^{-1} cube face are all larger by about 0.027 to 0.235 than their corresponding values on the 0.2 mol L^{-1} face. Similar arguments using the other faces of the cube allow analysis of the effects of both peak separation ΔE and $|I_{pa}/I_{pc}|$ current ratio, and are useful for obtaining a physical interpretation of the type of electrolyte and surface main effects for ΔE and $|I_{pa}/I_{pc}|$.

The factorial design diagram shown in Figure 5 is also useful for choosing the optimized experimental conditions. If only peak separation is considered, the best set of conditions from the factorial study is − − + (20 mV s^{-1}, KCl, 1.0 mol L^{-1}) indicating that the pH level does not affect ΔE. Values of $|I_{pa}/I_{pc}|$ close to unity are found for the following sets of conditions − − + (20 mV s^{-1}, KCl, 1.0 mol L^{-1}) and − + + (20 mV s^{-1}, CH_3COONa, 1.0 mol L^{-1}) showing that aqueous phase pH is also not relevant for $|I_{pa}/I_{pc}|$. These conditions are therefore recommended to achieve most reversible behaviour.

4. Conclusions

Organic dye TB^+ was immobilized onto SiO_2/Sb_2O_3 prepared by the sol–gel method. Carbon paste modified with this material having dye immobilized on its surface showed high chemical stability attributable to the strong adsorption of dye on the matrix. The full factorial design used here allows a simultaneous investigation of four selected factors that affect the optimization of reversibility characteristics of the adsorbed mediator dye.

In the factorial design study the aqueous phase pH factor did not influence either the peak separation response ΔE, or the $|I_{pa}/I_{pc}|$, current ratio response. If only peak separation is considered, the best set of conditions from the factorial study is $- - +$ (20 mV s^{-1}, KCl, 1.0 mol L^{-1}) indicating that the pH levels do not affect ΔE. Values of $|I_{pa}/I_{pc}|$ close to unity are found for the sets of conditions $- - +$ (20 mV s^{-1}, KCl, 1.0 mol L^{-1}) and $- + +$ (20 mV s^{-1}, CH_3COONa, 1.0 mol L^{-1}) showing that the aqueous phase pH factor is not relevant and therefore does not affect $|I_{pa}/I_{pc}|$.

Acknowledgements

Y.G. and R.E.B. are indebted to FAPESP and CNPq for financial support. E.S.R. and S.T.F. are indebted to FAPESP, S.L.P.D. is indebted to CAPES-PICDT for fellowships.

References

1. G. Zaitseva, Y. Gushikem, E.S. Ribeiro and S.S. Rosatto, *Electrochim. Acta* **47** (2002) 1469.
2. X.T. Gao, J.L.G. Fierro and I.E. Wachs, *Langmuir* **15** (1999) 3169.
3. V. Menon, V.T. Popa, C. Contescu and J.A. Schwarz, *Rev. Roum. Chim.* **43** (1998) 393.
4. J.M. Miller and L.J. Lakshmi, *J. Phys. Chem. B* **102** (1998) 6465.
5. H. Kochkar and F. Figueras, *J. Catal.* **171** (1997) 420.
6. D.C.M. Dutoit, M. Schneider, P. Fabrizioli and A. Baiker, *J. Mater. Chem.* **7** (1997) 271.
7. A.M. Castellani and Y. Gushikem, *J. Colloid Interface Sci.* **230** (2000) 195.
8. J.E. Gonçalves, Y. Gushikem and S.C. de Castro, *J. Non-Cryst. Solids* **260** (1999) 125.
9. A. Walcarius, *Electroanalysis* **10** (1998) 1217.
10. C.U. Ferreira, Y. Gushikem and L.T. Kubota, *J. Solid State Electr.* **4** (2000) 298.
11. H. Galip, H. Hasipoglu and G. Gunduz, *J. Appl. Polym. Sci.* **74** (1999) 2906.
12. H. Sato, K. Kondo, S. Tsuge, H. Ohtani and N. Sato, *Polym. Degrad. Stabil.* **62** (1998) 41.
13. H.C. Jung, W.N. Kim, C.R. Lee, K.S. Suh and S.R. Kim, *J. Polym. Eng.* **18** (1998) 115.
14. P. Carty and W. White, *Polym. Degrad. Stabil.* **47** (1995) 305.
15. M. Nalin, M. Poulain, S.J.L. Ribeiro and Y. Messaddeq, *J. Non-Cryst. Solids* **284** (2001) 110.
16. U.A. Schubert, F. Anderle, J. Spengler, J. Zuhlke, H.J. Eberle, R.K. Grasselli and H. Knozinger, *Top. Catal.* **15** (2001) 195.
17. J.H. Youk, R.P. Kambour and W.J. MacKnight, *Macromolecules* **33** (2000) 3594.
18. H.F. Zanthoff, W. Grunert, S. Buchholz, M. Heber, L. Stieveno, F.E. Wagner and G.U. Wolf, *J. Mol. Catal. A-Chem.* **162** (2000) 435.
19. V.P. Vislovskiv, V.Y. Bychkov, M.Y. Siney, N.T. Shamilov, P. Ruiz and Z. Schay, *Catal. Today* **61** (2000) 325.
20. C. Janardanan and S.M.K. Nair, *Indian J. Chem.* **31A** (1992) 136.
21. C. Janardanan and S.M.K. Nair, *Analyst* **115** (1990) 85.
22. L.T. Kubota, F. Gouveia, A.N. Andrade, B.G. Milagres and G. Oliveira Neto, *Electrochim. Acta* **41** (1996) 1465.
23. E.F. Perez, G. Oliveira Neto and L.T. Kubota, *Sensors Actuators B* 72 (2001) 80.
24. J.M. Ottaway, *in* A.J. Bard (Ed.), 'Indicators' (Pergamon, Oxford, 1972), pp. 469–529.
25. L. Gorton, A. Tortensson, H. Jaegfeldt and G. Johansson, *J. Electroanal. Chem.* **161** (1984) 103.
26. Q. Chi and S. Dong, *Electroanalysis* **7** (1995) 147.
27. A. Malinauskas, T. Ruzgas and L. Gorton, *J. Electroanal. Chem.* **484** (2000) 55.
28. C.A. Pessoa, Y. Gushikem, L.T. Kubota and L. Gorton, *J. Electroanal. Chem.* **431** (1997) 23.
29. C.A. Pessoa, Y. Gushikem and L.T. Kubota, *Electroanalysis* **9** (1997) 800.
30. A. Walcarius, *Electroanalysis* **13** (2001) 701.
31. B. de Barros Neto, I.S. Scarminio and R.E. Bruns, *in* '*Como fazer experimentos*: *Pesquisa e Desenvolvimento na Ciência e na Indústria*', (Editora da UNICAMP, Campinas-SP, Brazil, 2001).
32. G.E.P. Box, W.G. Hunter and J.S. Hunter, 'Statistics for experiments', (Wiley, New York, 1978).
33. 'Statistica for Windows', VERSION 5.0 (Statsoft, Inc., Tulsa, OK, 1995).
34. A.A. Ensofi, T. Khayamian and B. Hemmateenejad, *Anal. Lett.* **32** (1999) 111.
35. R.F. Rocha, S.S. Rosatto, R.E. Bruns and L.T. Kubota, *J. Electroanal. Chem.* **433** (1997) 73.
36. M.E.P. Hows, D. Perrett and J. Kay, *J. Chromatogr. A.* **768** (1997) 97.
37. P.J. Goodhew and F.J. Humphreys, '*Electron Microscopy and Analysis*', 2nd edn (Taylor & Francis, London, 1992).
38. J.A. Bearden, *Ver. Mod. Phys.* **39** (1967) 78.
39. L. Antonov, G. Gergov, V. Petrov, M. Kubista and J. Nygren, *Talanta* **49** (1999) 99.
40. D.D. Schlereth and A.A. Karyakin, *J. Electroanal. Chem.* **395** (1995) 221.
41. P.D. Atkins, '*Physical Chemistry*', 6th edn (OUP, Oxford, 1998).